Acoustic Emission Analysis of Experimental Impact Processes in Comparison to Ultrasound Measurements and Numerical Modeling

Dorothee Moser[1], Nicole Güldemeister[2], Kai Wünnemann[2] and Christian Grosse[1]
[1]Technische Universität München, Chair of Nondestructive Testing, München, Germany
[2]Museum für Naturkunde, Leibniz Institute for Research on Evolution and Biodiversity, Berlin, Germany

Abstract

In this paper we present acoustic emission (AE) data recorded in hypervelocity impact experiments. In particular we focus on the presentation of the experimental setup and the data analysis. The AE data are used to localize the impact point, to analyze the propagation of the compressive wave in the target, and to calibrate specific material properties under dynamic conditions required in numerical simulation of impact cratering and the propagation of shock waves. We present a detailed comparison between experimentally determined data and numerical models. Additionally, we measured the wave velocity of the material with ultrasound tomography before the impact and compare the expected travel time of the compressional wave at each sensor with the arrival time of the compressional wave recorded by AE technique during an experiment under dynamic conditions. We recorded the stress signal in numerical models at gauges that were located at exactly the same positions as the AE sensors. A good agreement has been found between experimentally and numerically determined wave speeds. The impact experiments provide information about wave propagation that may contribute to a better understanding of the generation of earthquake-like seismic waves during the hypervelocity impact of a meteorite on earth. The calibration of numerical models is of particular importance for the up-scaling of the experimental results.

1. Introduction and Motivation

The generation and growth of fractures during a hypervelocity impact and the propagation of elastic-plastic waves are not yet sufficiently investigated. Hypervelocity impact experiments are limited in terms of the data that can be recorded and the characterization of processes during impact. Several non-destructive testing methods have been used to characterize ongoing processes such as the generation, propagation of shock waves, their attenuation into elastic waves, and permanent modifications in the target material caused by an impact. During an impact event a shock wave is generated that propagates through a target material. Due to compression of the material a great part of the initial impact energy is converted into plastic work. Thus, the shock wave attenuates with distance and eventually turns into elastic waves. Here we present complex measurements of the resulting elastic waves using AE during impact experiments to determine material parameters, the compressional wave propagation in the target, to quantify fracturing in the target, as well as the localization of the impact. Additionally, measurements with elastic waves (ultrasound) were conducted before the impact experiments to calculate the expected wave propagation in the target.

In the framework of the DFG project “MEMIN” (multidisciplinary experimental and modeling impact crater research network), laboratory impact experiments have been carried out to generate impact crater structures on the decimeter scale (Kenkmann et al. 2011, Poelchau et al. 2013, Moser et al. 2013, Lexow et al. 2013, Hoerth et al. 2013). The experiments were aimed at simulating natural meteorite impacts on planetary surfaces and on Earth. The impact process was

analyzed to address different aspects such as the resulting crater morphology and morphometry, the crushing of pore space in the target material by the generated shock wave and the reconstruction of the ejecta (Buhl et al. 2013, Ebert et al. 2013, Sommer et al. 2013, Dufresne et al. 2013, and Kowitz et al. 2013). Non-destructive testing methods are suitable to visualize the damage zone underneath the crater (Moser et al. 2013) and the here discussed wave propagation induced by the impact. An important complementary method to analyze impact processes and the generated wave propagation is numerical modeling. To achieve realistic results, enabling valid material prognoses, calibration and validation of numerical models is required. This can be done by using AE and other non-destructive testing techniques.

Here we present the setup for dynamic AE measurements during hypervelocity impact experiments in a laboratory chamber under vacuum conditions. Moreover, we describe how to record the AE and how to analyze the data. In order to improve the characterization of the properties of the target material, we conducted travel time measurements with static ultrasound through-transmission techniques prior to the impact experiments (for more details see Moser et al. 2013). In addition, numerical modeling is used to simulate the propagation of waves and compare the results with experimental observations (Güldemeister et al. 2013a). The main difference of the two types of target material (quartzite and sandstone) is porosity, which poses a challenge in modeling the material behavior under highly dynamic conditions. The unique data set obtained from the given experiments was used to validate and calibrate material models in hydrocode simulations against static observations (ultrasound tomography) and dynamic measurements of the acoustic signal (AE). The combination of an AE technique and numerical modeling of crater formation and wave (shock, plastic, elastic) propagation in the impacted target will further our understanding of wave propagation in nonporous and porous materials. The development and improvement of material models will improve the applicability of numerical models to upscale the results from the laboratory scale to the scale of natural impact craters as a next step of research.

2. Methods

Non-destructive measurements in the MEMIN project are used to obtain quantitative data of the damage inside the impacted targets. The present AE technique records elastic wave signals generated by the impact in the experiments to gain information about the exact position of the point of impact and the fracturing process. Additional methods (ultrasound tomography, microcomputer tomography, modal analysis and phase spectroscopy) are used to investigate the characteristics and quality of the target before the impact. After the impact the same methods are used to map the extent and degree of damage below the crater structure (Moser et al. 2013).

All laboratory impact experiments are carried out in the facility of the Ernst Mach Institute in Freiburg (Germany). The experiments simulate meteoritic impacts at a surface like the earth. Iron meteorite, steel and aluminum projectiles, ranging in sizes from 2.5 to 12 mm, were accelerated with a two-stage light gas gun to velocities of 2500 to 7800 m/s. The projectile impacted in sandstone (Seeberger Sandstein), tuff or quartzite targets producing craters of 5 to 29 cm in diameter (Poelchau et al. 2013, Heorth et al. 2013). The investigated target is positioned in a chamber that was evacuated to a pressure of around 100 mbar (Poelchau et al. 2013). The evolution of the damage zone and wave propagation in the target material has been investigated using non-destructive techniques such as AE and ultrasound tomography (Moser et al. 2013), and by numerical modeling (Güldemeister et al. 2013b).

Here we refer to experiments with 20 cm cubed quartzite, sandstone and tuff targets and a projectile size of 2.5 mm impacting at 4500 m/s. For the comparison with numerical modeling results, we additionally consider an experiment with a 50 cm cubed sandstone target and a projectile of 10 mm in diameter. The sandstone has an initial porosity of 25 %.

The AE technique as well as numerical models are making use of sensors (gauges) attached to the target surface. The location of the sensors was chosen to ensure a broad coverage over the target on all sides (Fig. 1). To make the recorded seismic signals in the numerical models and the experiments directly comparable it is important to choose the same locations for the sensors in experiment and model. As the target has the geometry of a cube in the experiments, but a cylindrical geometry in the numerical models it was only possible to measure the seismic signals at similar distance but not at exactly the same location. We determined the point in time of the first arrival of the elastic wave in experiment and model at each sensor. The wave velocity is then given by the distance and the elapsed time and can be determined for the different materials at each sensor (Güldemeister et al. 2013b).

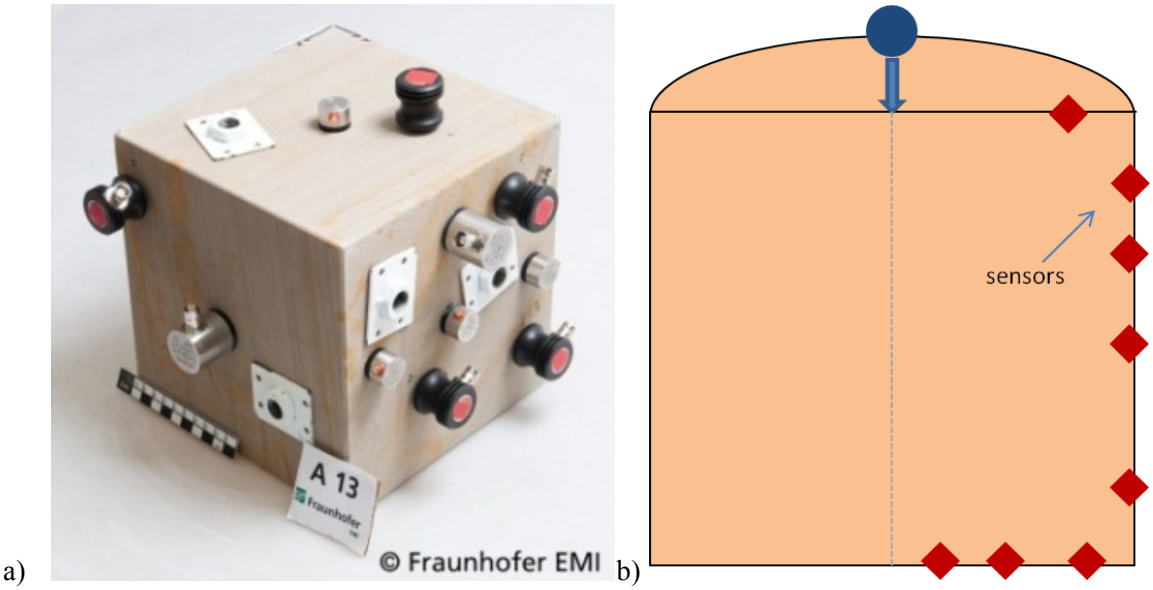

Fig. 1. Experimental and numerical setup. a) Setup of sensors and sandstone target for the AE experiment before the impact. b) Numerical setup of the target block with sensors. The numerical model uses a cylindrical target whereas the experimental target is represented by a cube.

2.1 Acoustic emission techniques

Acoustic emission techniques (AET) are considered to be quite unique among the non-destructive testing (NDT) methods. In contrast to other NDT methods, AET is usually applied during loading, whereas most others are applied before or after loading of a structure, as it is the case for the ultrasound method. The ultrasound method is an NDT technique, which is able to detect the geometric shape of a defect in a specimen using an artificially generated source signal and a receiver. In contrast AET detect the elastic waves radiated by a growing fracture. It is useful to compare the results of AE tests with other NDT methods, such as ultrasound (tomography, see below) or numerical modeling.

Acoustic emission can be considered to be a form of microseismicity, comparable to earthquakes. AE is defined as the spontaneous release of localized strain energy in stressed

material. An amount of energy is released due to microcracking or friction, which can be recorded by transducers (sensors) on the materials surface. AE testing is similar to seismological techniques – they basically use the same approach but at a different scale. In contrast to both, far-field seismology, which investigates earthquakes at a distance of thousands of kilometers, as near-field seismology for several hundred kilometers, AET are usually applied for several tenths of meters down to millimeters. For the present impact cratering experiments the current distance is up to several decimeters.

Seismological data are usually analyzed on the basis of their full waveform or of a significant part of it. For AET the waveform is not expedient in every occasion, and its use depends on the type of application. For example, the disruption of the recording of waveforms through restrictions of electronic components could interfere. In these cases only certain parameters are extracted from the signals and stored away in the memory. Nowadays these parameter-based techniques are often combined with so-called signal-based recording techniques (as summarized in Grosse & Ohtsu 2008). A first report goes back to the late 1980's and the early 1990's (Sachse & Kim 1987; Ono 1994). Seismological data analysis techniques were adapted for the investigation of failure processes in concrete by for example Ouyang et al. (1991) and Ohtsu et al. (1991). The basis for this development is the advances in microelectronics and in computer-based recording techniques. AE usually deals with high signal rates and events at relatively high frequencies (from 20 kHz up to several MHz). Modern devices are able to handle such a type of data enabling for techniques such as the localization of AE events or moment tensor inversion.

A major advantage of AE techniques is the ability to observe dynamic processes, which is not the case for most other non-destructive testing techniques. Results can be visualized in 4D (geometry and time) for deterioration processes like impacts, which are used in this study to investigate the cratering process.

2.2 Ultrasound tomography before impact

The velocity of the wave propagating through the material significantly depends on the characteristics of the impact materials and has a constant elastic wave velocity (Pilkington & Grieve 1992, Ahrens & Rubin 1993; Xia & Ahrens 2001, Ai 2006). However affected by stratification or damage, the compressional wave velocity of a material can be highly influenced by the inhomogeneity of a target. Hence, observed and measured wave velocity give important insights into material processes during and after an impact event.

The characterization of the compressional wave velocity inside a target can be achieved by ultrasound (US) through-transmission measurements. A three dimensional resolution with recordings from every surface with a specified measurement grid is possible. In a homogeneous material the mean wave velocity of every ray path is constant for transmission measurement with ultrasound sensors. Fractures and cracks as well as bedding in the probed materials determine a variable reduction of the mean wave velocities according to the crack and bedding quantity, density, dimension, and orientation. The mesh grid of the ultrasound tomography has a limited resolution (here 1 cm) but are deeply influenced by a high micro-crack density (Pilkington and Grieve 1992). The wave velocity for sandstone, quartzite, and tuff was measured in each spatial direction before the impact as presented in Table 1 (only the mean wave velocity for each direction is shown). Usually, the experimental impact surface was horizontal related to the bedding (y-z plane). Thus, the wave velocity is also dependent on the bedding. With the measured travel times of the compressional wave in each direction, the wave propagation and the wave velocity can be described by the slope in Fig. 2.

The results of the ultrasound measurements are only used to compare them with the results of the AE and the numerical models. The description of the method (Moser et al. 2013) is not important for the discussion of the AE results.

Table 1 The mean wave velocity in [m/s] for three different targets in each spatial direction, measured with ultrasound. The sandstone with 50 cm edge lengths (values measured with US only in the center of each surface) and quartzite and tuff with 20 cm edge lengths (values measured in a 1 cm grid with US, given is the calculated mean value).

Target material	**x-y**	**x-z**	**y-z**
Sandstone (D1)	3000 ± 10	3050 ± 10	2850 ± 10
Quartzite (A22)	4500 ± 100	4950 ± 60	5000 ± 80
Tuff (A25)	2050 ± 30	2150 ± 50	2100 ± 60

All values are given in m/s.

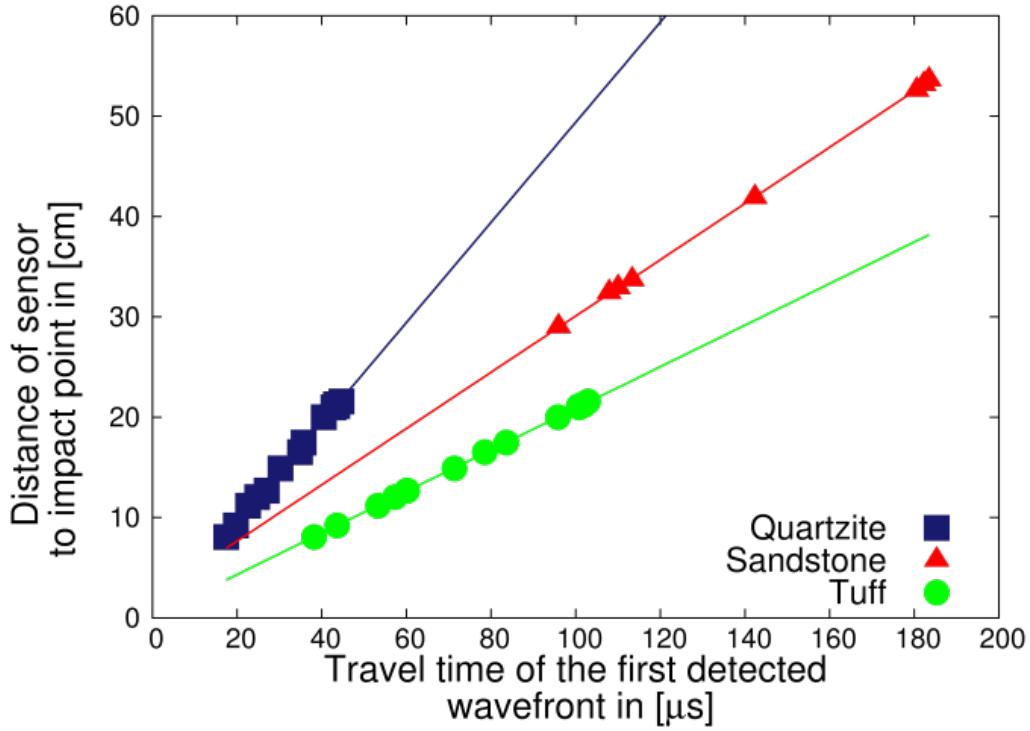

Fig. 2. The wave propagation for a quartzite target (blue symbols) with a mean wave velocity of 5000 m/s, sandstone targets (red symbols) with a mean wave velocity of 2.8 km/s, and tuff (green symbols) with a mean wave velocity of 2100 m/s. The velocities have been determined from the slope of a line fitted to the data assuming a constant wave speed. The targets had block sizes of 20 cm edge lengths for quartzite and tuff, and 50 cm edge lengths for sandstone.

2.3 Numerical modeling

For the simulations of impact experiments we used the multi-material, multi-rheology hydrocode iSALE (Elbeshausen et al. 2009, Wünnemann et al. 2006), which includes an elasto-plastic constitutive model (Collins et al. 2004) describing the mechanical response of rocks to deformation.

To describe the thermodynamic behavior of the material we made use of the Analytical Equation of State (ANEOS, Thompson and Lauson 1972) for quartzite (Melosh 2007). In case of

a porous sandstone target the ANEOS has been combined with the ε-a compaction model (Wünnemann et al. 2006) to account for the effect of pore space crushing on shock wave propagation (Güldemeister et al. 2013a). The setup of the crater model was chosen similar to the experimental setup using approximately the same target dimensions, projectile and target properties and impact velocity. The porosity was set to 25 % comparable to the porosity of the sandstone used in the experiments. The projectile was represented by an ANEOS for iron. The model setup and material properties have been studied in previous work in detail (Güldemeister et al. 2013a). The study of the cratering process itself is not the objective of this work. Here we focus on the modeling of an experiment with a 20-cm cubed quartzite target and of a 50-cm cubed sandstone target and the recording of wave signals at a number of gauge points. In contrast to the experiments, where a rectangular block has been used as a target, we assumed a cylindrically symmetric geometry of the target in the models. This allows for simulating the experiments two-dimensionally with much lower computational demands. Due to the usage of a cylindrically symmetric grid, the location of the gauge points had to deviate from the location of the sensors in the experiment to keep the distance to the impact point the same. We considered the same number of gauge points as sensors in the experiments. The gauges/sensors were distributed at the impacted surface and at the backside of the target. We recorded different thermodynamic and mechanical parameters such as pressure and stress components as a function of time during wave propagation. We then picked the arrival time of the first detectable wave signal. A simplified model setup with the location of the gauge points is shown in Fig. 1b.

Additionally, we had to modify the material model due to the fact that wave velocity depends on porosity, which changes as a result of shock-induced crushing of pore space. The propagation of waves is significantly affected by the presence of porosity. The velocities in a porous material tend to be lower than in consolidated material. In the new model we assume a wave velocity for competent quartzite of 5000 m/s and for porous sandstone (25 % porosity) of 2900 m/s. These values have been obtained by ultrasound measurements. For intermediate porosities, as a result of different degrees of shock–induced crushing of pore space, we assume a linear dependency of wave velocity on porosity as wave velocities change with the crushing of open pore space.

3. Experimental setup for AE measurements

Two types of ultrasound sensors are used for the AET measurements (Fig. 3a and Fig. 4a). Both types of sensors are displacement sensors with piezo elements and have a broadband frequency spectrum (Fig. 3b and Fig. 4b). They were fixed at the surface of the target (Figs. 5a and b). A coupling agent was used to ensure a good contact between sensor and target. In the present experiments, we use superglue at the surface of the target for a smooth contact to the KRNBB-PC (Glaser-type) sensors (Fig. 4a). Additionally we used hot glue to adhere the Panametrics-NDT (V103) sensors (Fig. 3a) to maintain a better coupling effect between the sensor and the target surface. Since the energy induced by the impact is very high, the connection only with glue is not sufficient. For that reason the sensors are additionally fixed with screws and special fixtures at the target. Furthermore, we placed some sensors in boreholes of different depths at the backside of the impact surface. Therefore, special holders are constructed (Fig. 5c). For larger targets the sensors in the boreholes are at the backside of the impact surface in order to be closer to the impact.

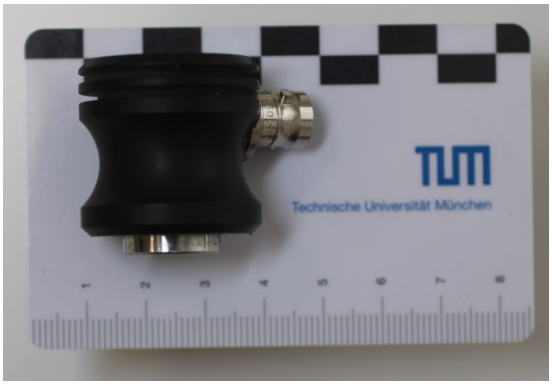

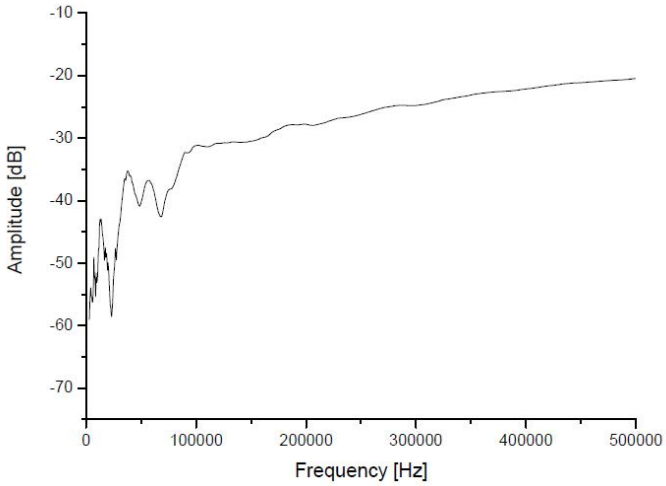

a) b)

Fig. 3. a) V103 ultrasound sensor with a relative big coupling surface (Ø = 1.4 cm). b) Frequency response of the V103 sensor (measured with the face-to-face method) (Richter 2009).

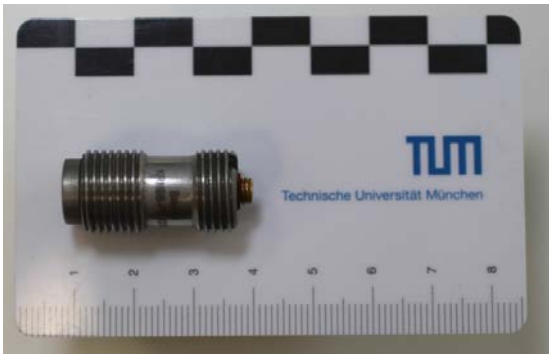

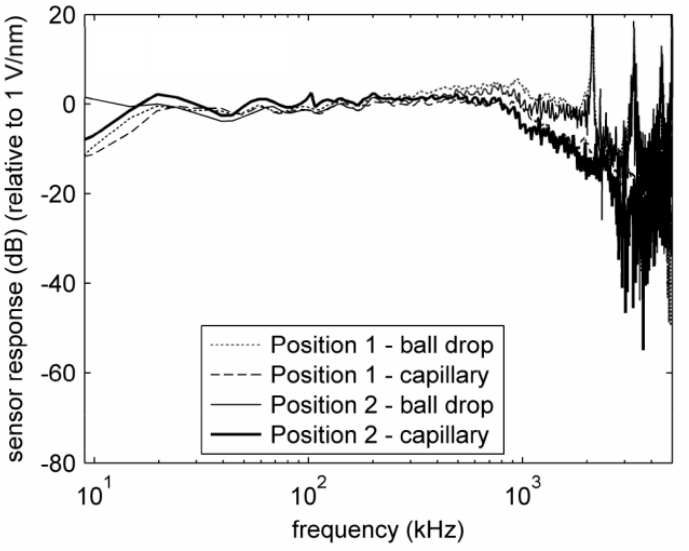

a) b)

Fig. 4: a) KRNBB-PC ultrasound sensor with a quasi-point coupling surface contact (~ 0.1 cm). b) Frequency response of the KRNBB-PC sensor for two different calibration sources (ruby ball drop and glass capillary fractures) (McLaskey2011).

To get as much information as possible the spatial distribution of the sensors is important. An asymmetrical distribution is favored to avoid and recognize problems with boundary and symmetric effects. The distribution for the laboratory experiments is changed partially for some experiments on a measurable scale. Table 2 shows an example of coordinates used for several experiments with 20-cm cubed targets. The origin of the coordinate system is shown in Fig. 6.

The sensors and the multi-channel transient recorder are connected with BNC coaxial cables (Figs. 5a and b). The transient recorder is a transportable computer with a measuring unit. Two measuring boards with respectively eight channels are able to connect overall 16 (AE) sensors for recording. Partially, a pre-amplifier is connected in series to optimize the signal to noise ratio. The amplifier enables a recording of signals over a large amplitude range. This phenomenon

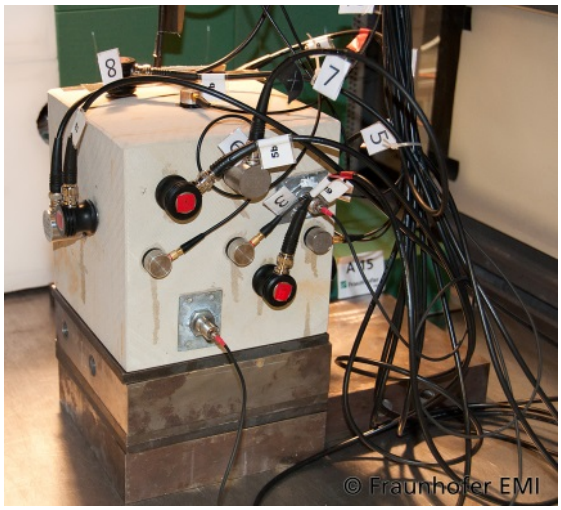

a)

b)


c)

Fig. 5: a) Target (20 cm cubed) inside the chamber of the light gas gun, including the sensors for the AE measurements at the surface. b) Setup of the experiment inside the chamber, including the target with sensors on the right and the ejector catcher on the left. The target-surface was marked with concentric rings of different colors equipped with trace elements to reconstruct the origin of the ejected target material. c) Special sensor-holder with sensor for boreholes.

Table 2: Example of sensor coordinates for the AE technique.

Sensor notation	**20cm target (x, y, z) cm**			**Sensor position**
A1	20	3	18	G, S
A2	0	16	15	G, S
A3	0	7	12	G, S
A4	14	15	20	G, S
A5	6	20	7	G, S
A6	15	0	9	G, S
A7	13	7	20	P, S
A8	0	20	17	P, S
B1	15	5	17	P, S
B2	16	4	5	P, S
B3	7	13	7	P, S

P = Sensor Panametrics, G = Sensor Glaser, S = Sensor position at the surface

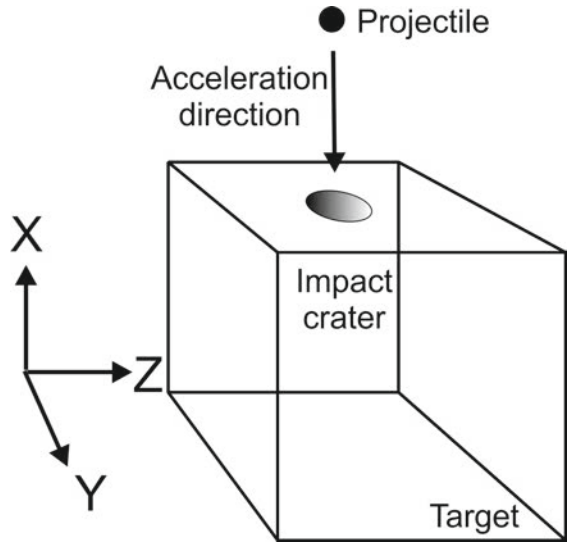

Fig. 6. Geometrical setup of the experimental target to show the origin of the coordinate system.

occurs due to the high energy of the impact. In contrast, the signals originating from cracks have much lower energies. For the recording of the AE signals of the impact experiment we utilize the *TransAs* system from *ELSYS AG*.

After instrumentation for AET, the setup has to be checked. Pencil leads were broken at the surface of the target at known coordinates (ASTM E 976-99, 1999). Therewith, the coupling of the sensors is secured and localization of the pencil leads is feasible. With these tests we get information about the quality of the algorithm to localize the impact as well as information about the wave propagation of the first detectable wave. If all recordings are satisfactory, the experimental chamber is closed and prepared for the hypervelocity impact experiment.

The recording of AE is started and ended manually. After setting the transient recorder to the record mode the room has to be vacated for security reasons. All measurements were recorded in a continuous mode so that the entire impact signal is saved as waveform data stream. After the shot of the projectile is performed, the recording was carried out for a time slot of about one minute. This time slot is important to get a chance to record some smaller events after the impact. It is necessary that there is no motion around the chamber, because the measurement technique is very sensitive to any movement. The recording of the data is at least three minutes: One minute before the experiment to prepare everything for the light gas gun, another minute after the shot without any moving around the experiment chamber and then it takes more or less a minute to return to the laboratory and to deactivate the measuring system. After the experiment, the tests with the pencil leads are repeated. This gives us information about changing velocities and therewith about fracturing inside the target.

4. Experimental and numerical results

4.1 Experimental results

The main goal of the AE measurements discussed in this paper is to localize the real impact point, as well as to reconstruct the propagation of the initial wave signal. The information to achieve these goals is given by the impact signal itself (Fig. 7). The arrival of the first detected elastic wave can be defined very well and a localization of the real impact point can be calculated. Also the velocity of the compressional wave can be calculated.

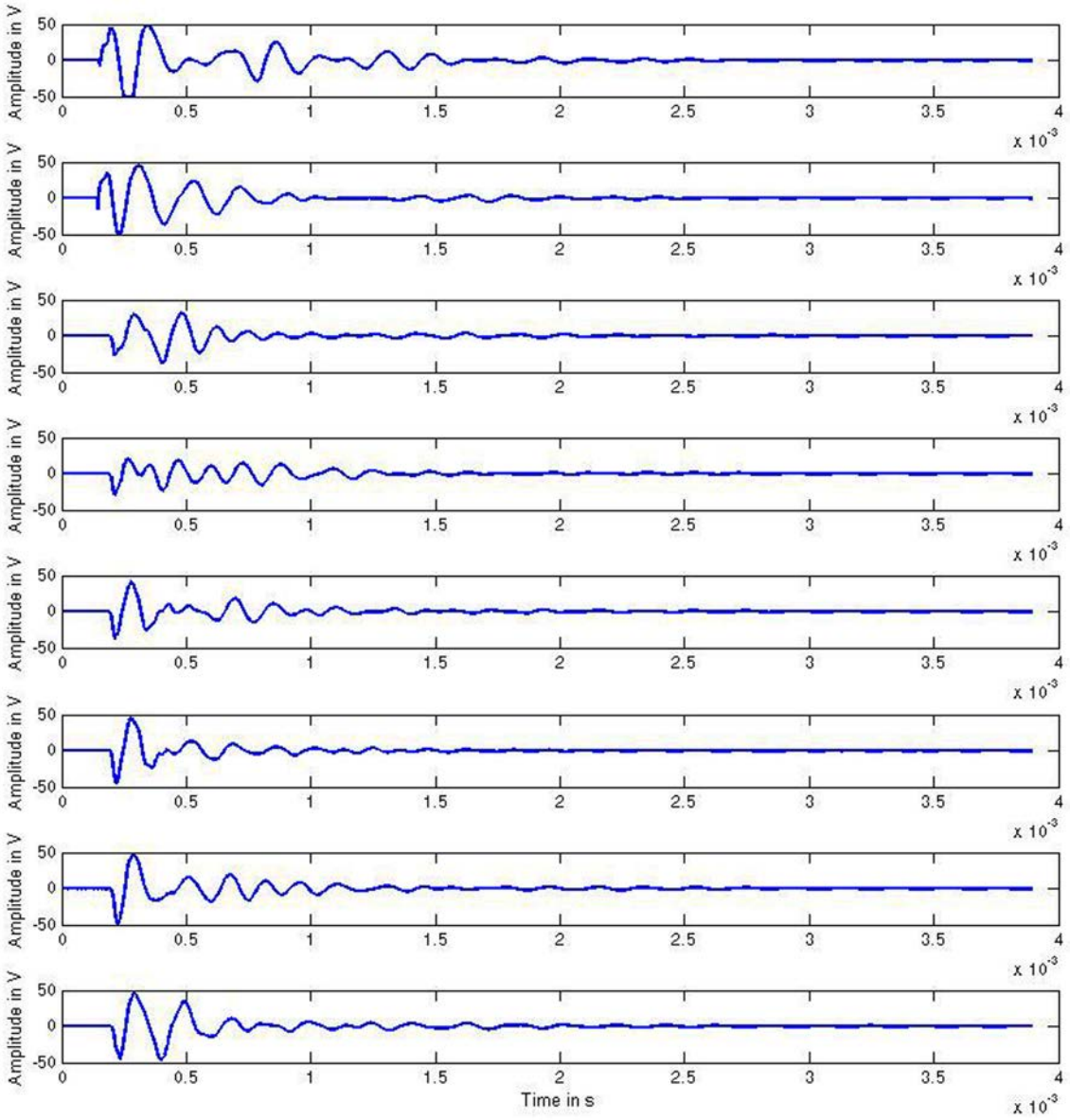

Fig. 7. Example of an original signal recorded by eight different sensors (V103) at an experiment with a 20-cm cubed sandstone target. The time slot shows 3 ms of the recorded signal with a detailed view at the time of the impact.

4.1.1 Localization: To determine the correct impact point we pick the first arrivals for each impact experiment with different target materials (17 x sandstone, 4 x tuff, and 3 x quartzite) and block sizes (15 cubes with 20 cm edge length, three cubes with 50 cm edge length, five cubes with 80 cm x 80 cm x 50 cm edge lengths, and one cube with 80 cm x 80 cm x 40 cm edge lengths). Figure 8 shows the localization of the impact points for six different 20-cm cubed targets. For comparison we used the midpoint of the crater structure, which was measured visually after the experiments. A good correlation between the localized impact point and the measured crater midpoint is observed. Only the calculated depths deviate from the measured midpoint on the surface. In that case, the impact point is calculated a few millimeters underneath the surface.

Figure 8 presents six experimental results, respectively two each of the sandstone, tuff and quartzite targets. For each experiment the AE localization results agree very well with the visually determined midpoint of the crater structure (deepest point of the crater structure). In Table 3 the impact points calculated using AE data are shown in comparison to the visually measured center of the crater. The x coordinate of the visually measured results is obtained by using an *Escan laser scanner* (Dufresne et al. 2013) and is much deeper than the localized impact point. This assumed that the projectile is penetrating forward after the first wave propagation is started. In y and z direction the deviations are less than 0.4 cm.

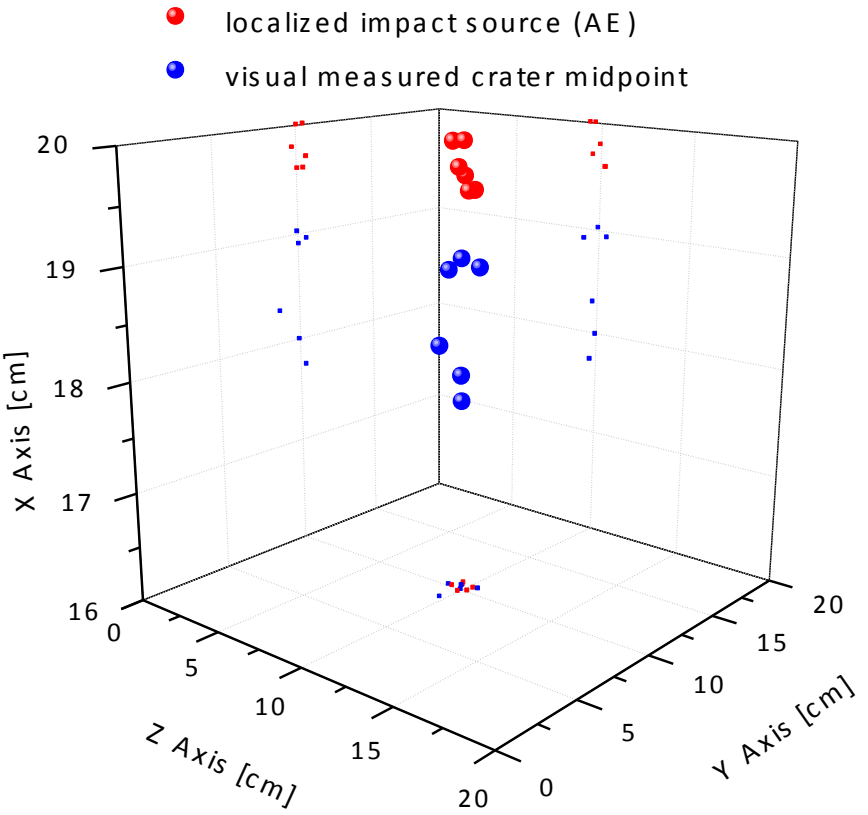

Fig. 8. Localization of six impact points of 20 cm cubed targets, respectively two sandstones, two quartzite, and two tuff targets. The red points show the localized impact points using AE data and the blue points represent the visually measured impact midpoints (bottom of the crater). The squares at the spatial sections are the projections of the impact points (all coordinates see Table 3).

4.1.2 Wave propagation: The travel time differences of the first recorded arrival at each sensor is also used to characterize the propagation of the compressional wave front (linear or more elliptical), and to analyze the compressional wave velocity of the material. The signals from AE experiments offer a velocity of 5000 m/s for the quartzite targets, 3.2 km/s for Seeberger sandstone and 2300 m/s for tuff (Fig. 9). These velocities were confirmed by the results of ultrasound (US) tomography measurements before the impact experiments for the same material (compare Table 1 and Fig. 2). The US tomography has a resolution of 1 cm and shows evenly distributed velocities for the targets. The compressional wave propagation also shows good linear propagation in all materials. The values of the expected wave velocity by US measurements and the recorded data of AE show differences of less than 14 % for each material (differences of all used methods are shown in Table 4). Figure 9 shows the recorded wave

(differences of all used methods are shown in Table 4). Figure 9 shows the recorded wave propagation for different target materials (two 20-cm cubed targets for quartzite and tuff, as well as a 50-cm cubed target for sandstone) where the time is plotted against the distance of the sensors. The measured variances of the velocity are probably related to the use of different measuring techniques (US tomography and AE) and by the fact that the assumed distance of impact and sensor has to be corrected. Here the midpoint of the sensor is used (the V103 sensors have a surface 1.6 cm in diameter) and the impact point is assumed at the surface almost directly above the deepest point in the crater structure. The localizations using the AE data show an impact source point above the surface. The wave propagation in the target induced by the impact, as well as the calculated wave propagation with the velocities measured by US technique shows a linear propagation.

Table 3: Coordinates of the localized impact points of 20 cm targets calculated with AE, visually measured and laser scanned.

Target	**x (AE)**	**Δx**	**y (AE)**	**Δy**	**z (AE)**	**Δz**	**x (S)**	**y (V)**	**z (V)**
A5 (sandstone)	19.8	0.2	9.8	0.2	10.0	0.1	18.83	8.8	10.2
A6 (sandstone)	20,0	0.5	10,1	0.4	9.4	0.4	18.9	10.1	9.2
A20 (quartzite)	19,6	0.4	10.5	0.2	10.3	0.3	18.94	10.6	10.5
A22 (quartzite)	19,6	0.3	10.1	0.1	10,3	0.2	19.02	10*	10*
A24 (tuff)	20,0	0.6	10.5	0.3	9,7	0.5	17.99	10*	10*
A25 (tuff)	119,7	0.6	10.7	0.3	9.6	0.5	17.73	10.3	9.9

All values are given in [cm]. **AE** = **AE**, **S** = laser **s**canned, **V** = **v**isually measured, **x – y – z** are the coordinates of the spatial directions, **Δx – Δy – Δz** are the calculated errors x, y and z, * no information about the real coordinates.

Table 4: Different wave velocities measured with ultrasound tomography, and AE, as well as calculated by numerical simulation.

Target material	**US**	**AE**	**N**
Tuff	2100	2300	n.m.
Sandstone	2800	3200	2900
Quartzite	5000	5000	4900

All values are given in m/s. **US** = **u**ltra**s**ound, **AE** = **a**coustic **e**mission, **N** = **n**umerical simulation, **n.m.** = **n**o **m**easurements

4.2 Numerical results

The time series of a recorded signal and the first detectable signal for three different sensors at different distances to the impact point for a quartzite and a sandstone target are shown in Fig. 10 (red line). Here, we concentrate on the first signal neglecting any subsequent usually much smaller signals. At all gauges and in all experiments the first signal is characterized by negative amplitude indicating a compressive wave. Note, we assume that negative stresses are compressive and positive stresses are tensile. It is further notable that the time series of the impact experiment in both targets show a distinct first signal.

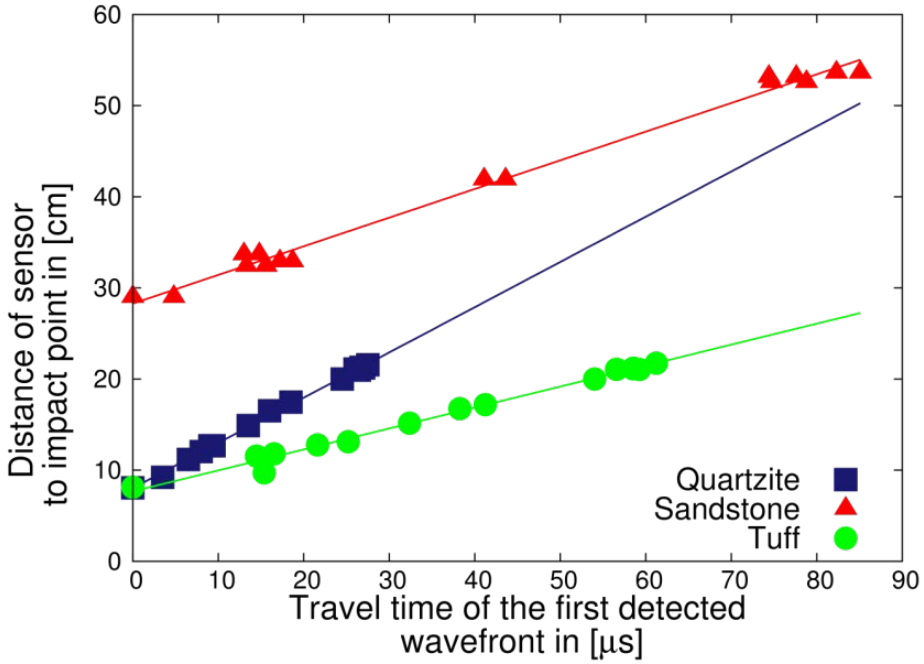

Fig. 9. Linear propagation of the first wave recorded at the AE sensors at the surface of the targets, normed at the first arrival of the sensor to the smallest distance to the impact point. A comparison between a quartzite (20-cm cubed target, 5000 m/s), sandstone (50-cm cubed target, 3200 m/s), and tuff target (20-cm cubed target, 2300 m/s) is shown. The sensor with the first signal recording is showing at the time of zero µs.

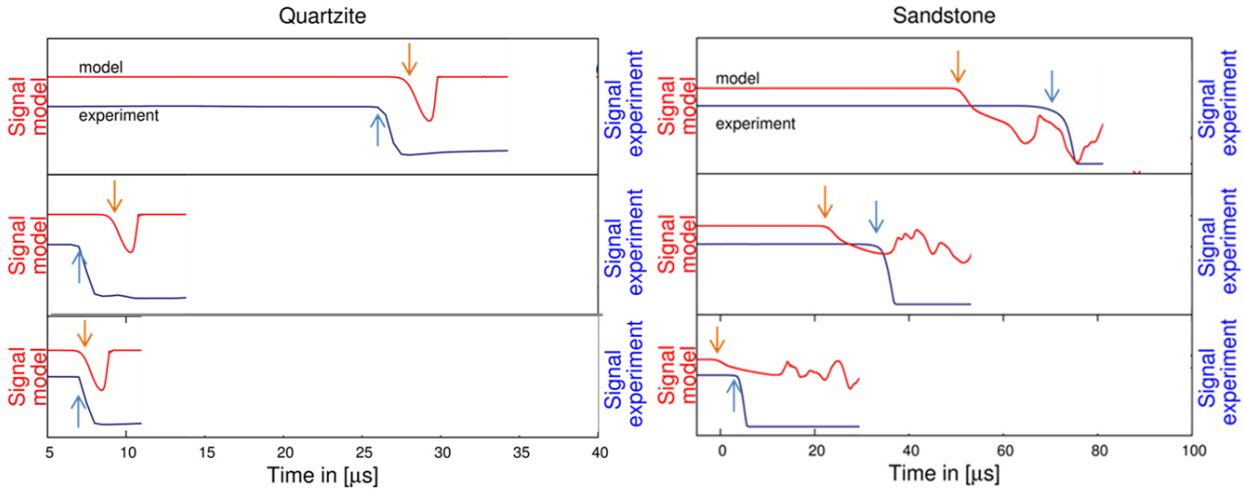

Fig. 10. Comparison of numerical and AE signals (measured with V103) of the first detectable wave signal recorded by three sensors of different distances to the impact point for quartzite (left) and sandstone (right). The distances of the sensors to the impact point increase from bottom to top. The arrows represent the point in time when the first detectable signal has been picked. Note the different scale on the x-axis due to fact that the quartzite target is smaller (20 cm cubed) than the sandstone target (50 cm cubed). The AE signals have been clipped.

We picked the first arrival times of the impact-induced waves at each gauge point in the numerical models with quartzite and sandstone and plotted the time versus distance to the impact point in Fig. 11. We obtained a wave velocity from the slope of a line fitted to the modeled data assuming a constant wave speed. We find a velocity of 4900 m/s for the quartzite target and 2900 m/s for the sandstone target. The quartzite and sandstone velocities agree with the speed of sound of the elastic wave from the ultrasound measurements (5000 m/s and 2800 m/s respectively). Additionally, we note that the propagation of the wave and therefore the determined wave velocities are porosity-dependent resulting in a significantly reduced propagation velocity of the elastic wave.

4.3 Comparison of experiment and numerical model

In general, the experimental and numerical results of the wave velocities are in excess of the US velocity measured before the experiment (compare Table 1). The experimentally obtained wave velocity of 5000 m/s for quartzite is in good agreement with the numerically determined velocity of 4900 m/s. For the sandstone target, the velocity determined by AE (3200 m/s) deviates slightly from the numerical model (2900 m/s). Figure 11 shows the comparison of the linear propagation of the first wave front inside the target for the experiment and the model.

A comparison of the numerical and experimental time series for quartzite and sandstone is shown in Fig. 10. Generally, a good agreement between the numerical models and the experimental data considering the arrival times and the signal phase is observed. Note, that the experimental data have been capped due to overdriving and that we only record the first signal that arrives.

In summary, we are able to reproduce first-arrival-times in non-porous quartzite in the numerical models and are able to show a reduced velocity of the elastic wave for porous material (sandstone) as shown in the experiments. However, the determined velocity is about 10 % above the measured velocity in the experiment.

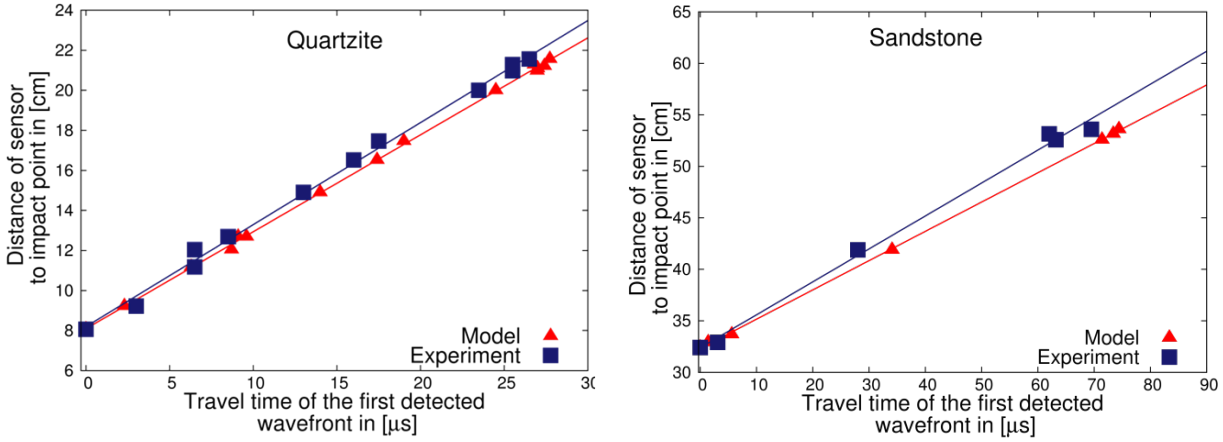

Fig. 11. Linear propagation of the first wave front inside the target for the experiment and the model. The plot shows the distances of different sensors dependent on the arrival time. The average wave velocity is measured to be around 5000 m/s (experiment) and 4900 m/s (model) for quartzite (left) and 3200 m/s (experiment) and 2900 m/s (model) for sandstone (right). Please note the different block sizes and thus scale on the x-axis. For the quartzite a 20-cm cubed target has been used, for the sandstone a 50-cm cubed target.

5. Discussion

By means of laboratory cratering experiments we demonstrate that the recording of AE during impact events is possible. It was shown that the comparison of dynamic acoustic measurements and static measurements using ultrasound tomography regarding the elastic wave velocities is in principle possible. Small differences between static and dynamic measurements are due to the fact that (1) a shock wave that is initially generated travels at a higher speed and (2) crushing of pore space affects the propagation of elastic waves. We validated and calibrated numerical models against experimental results.

The measured wave velocities calculated by AE data agree very well with the results obtained by ultrasound through-transmission techniques as well as with the numerical results. Thus, the agreement between these techniques proved the applicability of the numerical models as well as the AE technique to investigate wave propagation in impact experiments (see Table 4, Figs. 10 and 11). Regarding the numerical modeling techniques, we are able to reproduce first-arrival-times in nonporous and porous target materials. The experimentally determined propagation velocities of the seismic signal during impact events agree well with numerical models. The propagation velocity of the elastic wave is reduced in porous material. In porous material the elastic properties change dynamically as porosity is crushed out by shock compression. We account for this effect by including a linear dependency of the wave velocity on porosity. The dependency of the wave velocity on porosity and other material parameters has to be investigated in more detail. Although experiments on the laboratory scale enable a good validation and calibration of numerical models against experimental observations, further improvements of our material model are required in particular for the behavior of porous materials.

Based on the determined wave velocities we were able to localize the exact point of impact. The reconstructed point of impact is in good agreement with the geometric center of the crater structure measured visually and by the laser scanning method by Dufresne et al. (2013) (compare to Table 3). The maximum deviation is 1.1 cm for all spatial directions. The highest deviation occurs in the direction of the impact. Based on AE techniques we locate the impact source much closer to the surface.

The experimental results were used to provide constraints to validate the material model which was partially successful but further improvements are necessary. So far, the numerical models agree with a homogeneous target material. A bedding of the target as shown by ultrasound measurements (Table 1) is not taken into account in the models. It still has to be considered that the targets have been measured with different measurement systems and under different conditions for different targets (ambient temperature, potential humidity, and bedding). Additionally, it was not possible to measure each target before the experiments to get the specific wave velocity.

In general, further improvements and refinements are necessary to further improve the agreement between experimental data and numerical models. However, the data we gained from the experiments provide a valuable benchmark for numerical models of shock wave propagation in porous material. The calibration of the material model against the AE data can now be used in simulations of natural meteorite impact events in sedimentary targets on the scale of several kilometers (Güldemeister et al. 2013b).

6. Conclusions

On the laboratory scale NDT methods are a valuable tool to determine target characteristics in terms of the elastic properties (wave velocity) before, during, and after hypervelocity impact experiments. The obtained data provide an important database as benchmark to validate numerical models against experimental observations. The combined experimental and numerical approach allows for up-scaling of the results from laboratory scale to the dimensions of natural impact craters. The major findings of this paper are:

1) The arrival of the elastic wave is measurable with acoustic emission. These dynamically obtained results verify static ultrasound measurements obtained before the impact event.

2) The experimentally determined wave propagation velocities of the seismic signal during impact events agree well with numerical models. Thus, the calibration and validation of numerical models is possible by using acoustic emission techniques. Further, wave velocities are reproducible for quartzite and sandstone. The propagation velocity of the elastic is reduced in porous material as shown by experimental and numerical measurements.

3) AE techniques enable further determination of the exact point of impact in hypervelocity impact experiments.

Acknowledgements

This research is part of the MEMIN program supported by the German Science Foundation DFG under Grant member FOR-887; GR 1664/6-1; WU 355／6-1.

References

T.J. Ahrens and A.M. Rubin (1993), Impact-induced tensional failure in rock. *Journal of Geophysical Research* 98, pp. 1185-1203.

H. Ai (2006), Shock-induced damage in rocks: Application to impact cratering. Ph.D. thesis, California Institute of Technology, Pasadena, California, USA, 159 p.

ASTM E 976-99 (1999). Standard Guid for Determinning the Reproducicility od Acoustic Emission Sensor Response. Techn. Ber.,American Society for Testing and Materials.

E. Buhl, M.H. Poelchau, G. Dresen and T. Kenkmann T. (2013), Deformation of dry and wet sandstone targets during hypervelocity impact experiments, as revealed from MEMIN program. *Meteoritics & Planetary Science* 48, pp. 71-86.

G.S. Collins, H.J. Melosh, and B.A. Ivanov (2004), Modeling damage and deformation in impact simulations. Meteoritics & Planetary Science 39, pp. 217–231.

A. Dufresne, M.H. Poelchau, T. Kenkmann, A. Deutsch, T. Hoerth, F. Schäfer and K. Thoma (2013), Crater morphology in sandstone targets: the MEMIN impact parameter study. *Meteoritics & Planetary Science* 48, pp. 50-70.

M. Ebert, L. Hecht, A. Deutsch and T. Kenkmann (2013), Chemical modification of projectile residues and target material in a MEMIN cratering experiment. *Meteoritics & Planetary Science* 48, pp. 134-149.

D. Elbeshausen, K. Wünnemann and G.S. Collins (2009), Scaling of oblique impacts in frictional targets: Implications for crater size and formation mechanisms. Icarus 204, pp.716–731.

C.U. Grosse and M. Ohtsu (2008), Acoustic Emission Testing in Engineering – Basics and Applications. Springer publ., Heidelberg , 410 p.

N. Güldemeister, N. Durr, K. Wünnemann and S. Hiermaier (2013a), Propagation of impact-induced shock waves in porous sandstone using mesoscale modeling. Meteoritics & Planetary Science 48, pp. 115-133.

N. Güldemeister, D. Moser, K. Wünnemann and C. Grosse (2013b), Recording the seismic signal generated by hypervelocity impact in experiments and numerical models. Lunar and planetary science conference 2013b, abstract #1474.
T. Hoerth, F. Schäfer, K. Thoma, T. Kenkmann, M.H. Poelchau, B. Lexow and A. Deutsch (2013), Hypervelocity impacts on dry and wet sandstone: Observations of ejecta dynamics and crater growth. *Meteoritics & Planetary Science* 48, pp. 23-32.
T. Kenkmann, K. Wünnemann, A. Deutsch, M.H. Poelchau, F. Schäfer and K. Thoma (2011), Impact cratering in sandstone: The MEMIN pilot study on the effect of pore water. *Meteoritics & Planetary Science* 46, pp. 890-902.
A. Kowitz, R.T. Schmitt, W.U. Reimold and U. Hornemann (2013), The first MEMIN shock experiments at low shock pressure (5-12.5 GPa) with dry, porous sandstone. *Meteoritics & Planetary Science* 48, pp. 99-114.
B. Lexow, M. Wickert, K. Thoma, F. Schäfer, M.H. Poelchau and T. Kenkmann (2013). The extra-large light-gas gun of the Fraunhofer EMI: Applications for impact cratering research. *Meteoritics & Planetary Science* 48, pp. 3-7.
G.C. McLaskey (2011), Stress Wave Source Characterization: Impact, Fracture, and Sliding Friction. Dissertation, University of California, Berkeley, 78 p.
H.J. Melosh (2007). Hydrocode equation of state for SiO_2. *Meteoritics & Planetary Science* 42, pp. 2035–2182.
D. Moser, M.H. Poelchau, F. Stark and C. Grosse (2013), Application of non-destructive testing methods to study the damage zone underneath impact craters of MEMIN laboratory experiments. *Meteoritics & Planetary Science* 48, pp. 87-98.
M. Ohtsu, M. Shigeishi, H. Iwase and W. Koyanagi (1991), Determination of crack location, type and orientation in concrete structures by acoustic emission. *Mag. Of Concrete Res.* Vol. 43, Nr. 155, pp. 127-134.
K. Ono (1994). Trends of recent acoustic emission literature. *Journal of Acoustic Emission* Vol.12, No. 3-4, pp. 177-198.
C. Ouyang, E.N. Landis and S.P. Shah (1991), Damage assessment in concrete using quantitative acoustic emission. *Journal Eng. Mech.* Vol. 117, No. 11: 2681-2697.
M. Pilkington and R.A.F. Grieve (1992), The geophysical signature of terrestrial impact craters. *Reviews of Geophysics* 30, pp. 161-181.
M.H. Poelchau, T. Kenkmann, K. Thoma, T. Hoerth, A. Dufresne and F. Schäfer (2013). The MEMIN research unit: Scaling impact cratering experiments in porous sandstones. *Meteoritics & Planetary Science* 48, pp. 8-22.
R. Richter (2009): Einsatz der Schallemissionsanalyse zur Detektion des Riss und Abplatzungs-verhaltens von Beton unter Brandeinwirkung. Diplomarbeit, Materialprüfungsanstalt Universität Stuttgart, 83 p.
W. Sachse and K.Y. Kim (1987). Quantitative acoustic emission and failure mechanics of composite materials. *Ultrasonics* Volume 25, 4, pp. 195-203
F. Sommer, F. Reiser, A. Dufresne, M.H. Poelchau, T. Hoerth, A. Deutsch, T. Kenkmann and K. Thoma (2013). Ejection behavior characteristics of experimental cratering in sandstone targets. *Meteoritics & Planetary Science* 48, pp. 33-49.
S. L. Thompson and H.S. Lauson (1972). Improvements in the Chart D radiation-hydrodynamic code 3: Revised analytic equations of state. Report SC-RR-71 0714. Albuquerque, New Mexico: Sandia National Laboratory. 119 p.
K. Xia and T.J. Ahrens (2001). Impact induced damage beneath craters. *Geophysical Research Letters* 28, pp. 3525-3527.